Chapter 3

Statistical analysis on MHD convective Carreau nanofluid flow due to bilateral non linear stretching sheet with zero mass flux condition *

3.1 Introduction

Stretching surface has intrigued many researchers due to its diverse applications in industrial and engineering fields like production of plastic and rubber plates, cooling of metallic plate in a bath, metal extrusion, etc. Both Newtonian and Non-Newtonian fluid flow over a bilateral non-linear stretching sheet has been studied by many researchers. MHD Carreau nanofluid flow over a bilateral stretching non-linear surface with zero mass flux condition has been studied in the chapter. Magnetic and heat source effects are accounted to analyse the effects of velocity and heat transport of Carreau nanofluid over a non linear stretching sheet. Effects of various parameters on skin friction coefficients and heat transfer rate are scrutinized using statistical techniques like slope of linear regression, correlation coefficient, probable error and regression.

3.2 Mathematical formulation

Three dimensional steady MHD Carreau nanofluid flow due to a bilateral stretching sheet with velocities $u_W = a(x+y)^m,\ v_W = b(x+y)^m;\ a,\ b,\ m > 0$ along the X and Y directions respectively is considered. Velocity, temperature and concentration equations are investigated with convective and zero mass flux condition at the

*Published in: Heat Transfer (Wiley), 2021; 50 (4) 3641-3660

surface. A non-uniform magnetic field $B = B_0(x+y)^{\frac{m-1}{2}}$ is applied along the Z direction (see Figure 3.1). In addition, a non-uniform heat generation or absorption $Q = Q_0(x+y)^{m-1}$ is implemented. The boundary layer equations (J. A. Khan et al., 2014), (Hayat, Aziz, et al., 2019) (M. Khan, Sardar, et al., 2018) are given by:

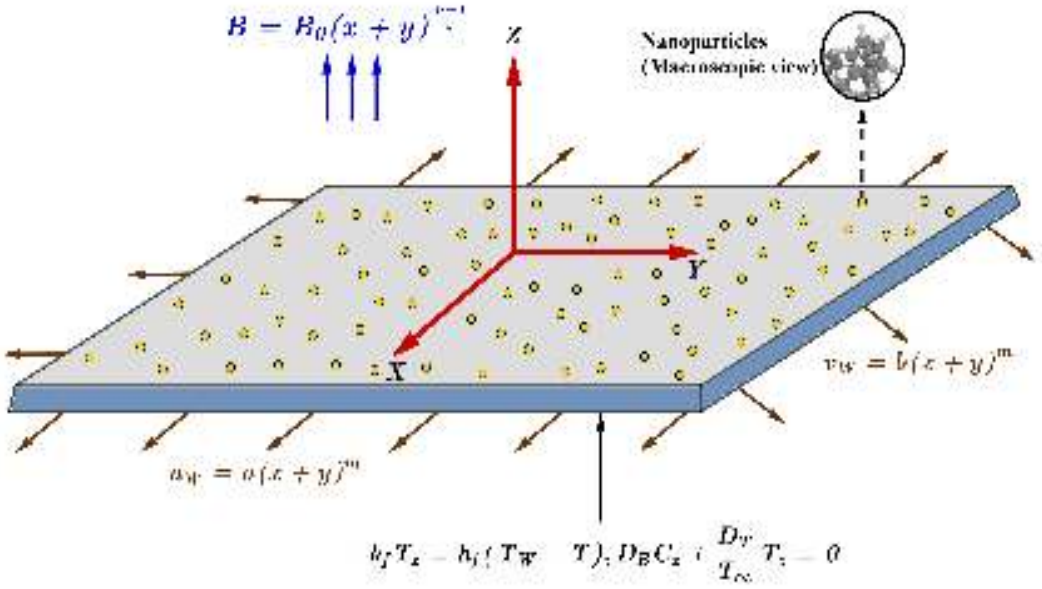

Figure 3.1: *Geometry of the problem*

$$u_x + v_y + w_z = 0 \tag{3.2.1}$$

$$\begin{aligned} uu_x + vu_y + wu_z = \nu_f u_{zz}\left[\beta^* + (1-\beta^*)\left\{1+\Gamma^2(u_z)^2\right\}^{\frac{n-1}{2}}\right] \\ +\nu_f\,(n-1)\,(1-\beta^*)\,\Gamma^2 u_{zz}(u_z)^2\left\{1+\Gamma^2(u_z)^2\right\}^{\frac{n-3}{2}} - \frac{\sigma B^2 u}{\rho} \end{aligned} \tag{3.2.2}$$

$$\begin{aligned} uv_x + vv_y + wv_z = \nu_f v_{zz}\left[\beta^* + (1-\beta^*)\left\{1+\Gamma^2(v_z)^2\right\}^{\frac{n-1}{2}}\right] \\ +\nu_f\,(n-1)\,(1-\beta^*)\,\Gamma^2 v_{zz}(v_z)^2\left\{1+\Gamma^2(v_z)^2\right\}^{\frac{n-3}{2}} - \frac{\sigma B^2 v}{\rho} \end{aligned} \tag{3.2.3}$$

$$uT_x + vT_y + wT_z = \alpha_f T_{zz} + \frac{Q}{(\rho c)_f}(T - T_\infty) + \tau\left[D_B T_z C_z + \frac{D_T}{T_\infty}(T_z)^2\right] \tag{3.2.4}$$

$$uC_x + vC_y + wC_z = D_B C_{zz} + \frac{D_T}{T_\infty} T_{zz} \tag{3.2.5}$$

The respective boundary conditions are given as:

$$\left.\begin{array}{c} u = u_W = a(x+y)^m, \quad v = v_W = b(x+y)^m, \quad w = 0 \\ -k_f T_z = h_f \left(T_W - T\right), \quad D_B C_z + \frac{D_T}{T_\infty} T_z = 0 \end{array}\right\} \text{ at } z = 0 \tag{3.2.6}$$

$$u \to 0, \quad v \to 0, \quad T \to T_\infty, \quad C \to C_\infty \quad \text{at } z \to \infty \tag{3.2.7}$$

The following similarity variables are implemented in converting the above system of partial differential equations into a system of ordinary differential equations:

$$\left.\begin{array}{c} u = a(x+y)^m \quad f'(\zeta) \\ v = a(x+y)^m \quad g'(\zeta) \\ w = -\sqrt{a\nu_f}\,(x+y)^{\frac{m-1}{2}} \quad \left[\ \frac{m+1}{2}\ (f(\zeta)+g(\zeta))\ +\ \frac{m-1}{2}\ \zeta\ (f'(\zeta)+g'(\zeta))\ \right] \end{array}\right\} \tag{3.2.8}$$

$$\theta(\zeta) = \frac{T - T_\infty}{T_W - T_\infty}, \quad \phi(\zeta) = \frac{C - C_\infty}{C_\infty}, \quad \zeta = \sqrt{\frac{a}{\nu_f}}\ z\ (x+y)^{\frac{m-1}{2}} \tag{3.2.9}$$

The transformed boundary layer equations are given below:

$$\begin{array}{c} f'''\left[\beta^* + (1-\beta^*)\left(1 + We^2 (f'')^2\right)^{\frac{n-3}{2}}\left(1 + nWe^2 (f'')^2\right)\right] - Mf' \\ -m(f')^2 - mf'g' + \frac{m+1}{2} f''(f+g) = 0 \end{array} \tag{3.2.10}$$

$$\begin{array}{c} g'''\left[\beta^* + (1-\beta^*)\left(1 + We^2 (g'')^2\right)^{\frac{n-3}{2}}\left(1 + nWe^2 (g'')^2\right)\right] \\ -Mg' - m(g')^2 - mf'g' + \frac{m+1}{2} g''(f+g) = 0 \end{array} \tag{3.2.11}$$

$$\theta'' + Pr\left[S\theta + Nb\phi'\theta' + Nt(\theta')^2 + \left(\frac{m+1}{2}\right)(f+g)\,\theta'\right] = 0 \tag{3.2.12}$$

$$\phi'' + \frac{Nt}{Nb}\theta'' + Sc\phi'\left(\frac{m+1}{2}\right)(f+g) = 0 \tag{3.2.13}$$

The corresponding boundary conditions are given by:

$$\left.\begin{array}{c} f(0) = 0, \quad g(0) = 0, \quad f'(0) = 1, \quad g'(0) = \delta \\ \theta'(0) = -Bi\left(1 - \theta(0)\right), \quad \phi'(0) + \frac{Nt}{Nb}\theta'(0) = 0 \end{array}\right\} \text{ at } z = 0 \tag{3.2.14}$$

$$f'(\infty) \to 0, \quad g'(\infty) \to 0, \quad \theta(\infty) \to 0, \quad \phi(\infty) \to 0 \tag{3.2.15}$$

where the non-dimensional parameters are taken as following:

$$\left.\begin{array}{c} We=\sqrt{\frac{\Gamma^2 a^3(x+y)^{3m-1}}{\gamma}},\quad M=\frac{\sigma B_o^2}{\rho_f a},\quad Pr=\frac{\nu_f}{\alpha_f},\quad Sc=\frac{\nu_f}{D_B},\quad \delta=\frac{b}{a} \\ Nt=\frac{\tau D_T(T_W-T_\infty)}{T_\infty \nu_f},\quad Nb=\frac{\tau D_B C_\infty}{\nu_f},\quad \tau=\frac{(\rho c)_p}{(\rho c)_f},\quad S=\frac{Q_0}{a(\rho c)_f} \end{array}\right\} \tag{3.2.16}$$

Skin friction coefficients, local Nusselt number and local Sherwood number measures the surface drag, heat transfer rate and mass transfer rate, respectively. They are defined (M. Khan et al., 2018), (Mahanthesh, Gireesha, & Gorla, 2017) as given below:(see Table 3.1)

3.3 Numerical solution

The equations (3.2.10) – (3.2.13) with boundary conditions (3.2.14)-(3.2.15) are solved numerically using bvp5c solver, a MATLAB built in function. To accomplish this, we choose:

$f=y_1,\quad f'=y_2,\quad f''=y_3,\quad g=y_4,\quad g'=y_5,$

$g''=y_6,\quad \theta=y_7,\quad \theta'=y_8,\quad \phi=y_9,\quad \phi'=y_{10}$

Accordingly, the equations (3.2.10) – (3.2.15) takes the form:

$$\begin{array}{c} y_1'=y_2,\quad y_2'=y_3,\quad y_3'=\frac{my_2^2+my_2y_5-\left(\frac{m+1}{2}\right)y_3(y_1+y_4)+My_2}{\beta^*+(1-\beta^*)\left(1+We^2y_3^2\right)^{\frac{n-3}{2}}\left(1+nWe^2y_3^2\right)} \\ y_4'=y_5,\quad y_5'=y_6,\quad y_6'=\frac{my_5^2+my_2y_5-\left(\frac{m+1}{2}\right)y_6(y_1+y_4)+My_5}{\beta^*+(1-\beta^*)\left(1+We^2y_6^2\right)^{\frac{n-3}{2}}\left(1+nWe^2y_6^2\right)} \\ y_7'=y_8,\quad y_8'=-\Pr\left[Sy_7+Nby_8y_{10}+Nt(y_8)^2+\left(\frac{m+1}{2}\right)(y_1+y_4)\,y_8\right],\quad y_9'=y_{10} \\ y_{10}'=\left\{\frac{Nt}{Nb}\ \Pr\left[Sy_7+Nby_8y_{10}+Nt(y_8)^2+\left(\frac{m+1}{2}\right)(y_1+y_4)\,y_8\right]-Scy_{10}\left(\frac{m+1}{2}\right)(y_1+y_4)\right\} \\ y_1(0)=0,\quad y_2(0)=1,\quad y_2(\infty)=0,\quad y_4(0)=0,\quad y_5(0)=\delta,\quad y_5(\infty)=0 \\ y_7(\infty)=0,\quad y_8(0)=-Bi\,(1-y_7(0)),\quad y_9(\infty)=0,\quad y_{10}(0)+\frac{Nt}{Nb}y_8(0)=0 \end{array} \tag{3.3.1}$$

Accuracy of the code and the validation of the current problem have been accounted through a restrictive comparison of the present work with prior published (J. A. Khan et al., 2014) results and is found to be in good agreement (described in Table 3.2).

3.4 Result and discussion

The impact of viscosity ratio parameter (β^*), Weisssenberg number (We), Hartmann number (M), heat generation/absorption parameter (S), power law index (n), Biot number (Bi), stretching ratio parameter (δ), Brownian motion parameter (Nb),

Table 3.1: *Skin friction coefficients, local Nusselt number and local Sherwood number are defined as given below:*

Local Nusselt number	$Nu = \frac{(x+y)q_w}{k_f(T_w - T_\infty)}$ where $q_w = -k_f\left(\frac{\partial T}{\partial z}\right)_{z=0}$
Reduced form of Nusselt number	$Re_x^{-\frac{1}{2}}\ Nu = -\theta'(0)$ where $Re_x = \frac{u_w(x+y)}{\nu_f}$ is the local Reynolds number along the x direction
Local Sherwood Number	$Sh = \frac{(x+y)m_w}{D_B(C_w - C_\infty)}$ where $m_w = -D_B\left(\frac{\partial C}{\partial z}\right)_{z=0}$
Reduced form of Sherwood number	$Re_x^{-\frac{1}{2}}\ Sh = -\phi'(0)$
Skin Friction Coefficients	$Cf_x = \frac{\tau_{zx}}{\rho_f u_w^2}$ where $\tau_{zx} = \mu_f\left(\frac{\partial u}{\partial z}\right)\left[\beta^* + (1-\beta^*)\left(1 + \Gamma^2\left(\frac{\partial u}{\partial z}\right)^2\right)^{\frac{n-1}{2}}\right]$
	$Cf_y = \frac{\tau_{zy}}{\rho_f v_w^2}$ where $\tau_{zy} = \mu_f\left(\frac{\partial v}{\partial z}\right)\left[\beta^* + (1-\beta^*)\left(1 + \Gamma^2\left(\frac{\partial v}{\partial z}\right)^2\right)^{\frac{n-1}{2}}\right]$
Reduced form of Skin Friction	$Re_x^{\frac{1}{2}} Cf_x = f''(0)\left[\beta^* + (1-\beta^*)\left(1 + We^2(f''(0))^2\right)^{\frac{n-1}{2}}\right]$
	$Re_y^{\frac{1}{2}} Cf_y = \delta^{-1.5}\ g''(0) \times \left[\beta^* + (1-\beta^*)\left(1 + We^2(g''(0))^2\right)^{\frac{n-1}{2}}\right]$ where $Re_y = \frac{v_w(x+y)}{\nu_f}$ is the local Reynolds number along y direction

thermophoresis parameter (Nt) on the X direction velocity ($f'(\zeta)$), Y direction velocity ($g'(\zeta)$), temperature ($\theta(\zeta)$) and concentration ($\phi(\zeta)$) profiles are carefully analysed through Figs. 3.2 - 3.13. The Prandtl number (Pr) and Schmidt numbers (Sc) are fixed at 5 and 2 respectively.

Table 3.2: *Comparison of* $f''(0)$ *and* $g''(0)$ *when* $\beta^* = 1$ *and* $M = 0$

m	δ	$f''(0)$ [Present paper]	$f''(0)$ (J. A. Khan et al., 2014)	$g''(0)$ [Present paper]	$g''(0)$ (J. A. Khan et al., 2014)
1	0	-1.000172394	-1	0	0
1	0.5	-1.22478775	-1.224745	-0.612393875	-0.612372
1	1	-1.414226121	-1.414214	-1.414226121	-1.414214
3	0	-1.624368157	-1.624356	0	0
3	0.5	-1.989423631	-1.989422	-0.994711816	-0.994711
3	1	-2.297186414	-2.297186	-2.297186414	-2.297186

Figs. 3.2 and 3.3 depict the variation of $f'(\zeta)$ and $g'(\zeta)$ due to the increment in β^*. The analysis has been carried out for shear-thinning n ($n < 1$) and shear thickening n ($n > 1$) cases. Both $f'(\zeta)$ and $g'(\zeta)$ exhibit an increase (shear-thinning case) with an increase in β^* whereas the results are reversed for the shear thickening case. The effect of We on $f'(\zeta)$ and $g'(\zeta)$ are elucidated in Figs. 3.4 and 3.5. A contrasting behaviour is observed on the velocity profiles for different values of n. An increase in We improves the elastic forces which hence causes a reduction in the velocity profiles in a shear-thinning fluid. Fig. 3.6 and 3.7 illustrates the variation of M on $f'(\zeta)$ and $g'(\zeta)$. An increment in M generates Lorentz force which retards $f'(\zeta)$ and $g'(\zeta)$ profiles. Fig. 3.8 exhibits the influence of δ on $g'(\zeta)$. As δ increases, $g'(\zeta)$ also increases since the vertical downward flow is accelerated due to the bi-directional stretching of the sheet.

With a rise in the magnitude of Bi, temperature profile is enhanced, shown in Fig. 3.9. Physically, this can be attributed to the fact that increase in Biot number enhances the heat transfer coefficient which in turn increases θ. Fig. 3.10 displays the effect of S on $\theta(\zeta)$. $\theta(\zeta)$ is observed to increase as S is increased. Fig. 3.11 reveals the change in $\theta(\zeta)$ with increasing Nt. Nt is found to have a positive effect. The mounting of Nt promotes an increment in the thermophoresis force which enforces the movement of nanoparticles from a hot region to a cold region and hence $\theta(\zeta)$ is increased. Fig. 3.12 describes the variation of $\phi(\zeta)$ with Nb. Nb shows a negative influence with $\phi(\zeta)$. Physically, an increase in Nb improves the random motion of nanoparticles which in return lowers the concentration of nanofluid. Fig. 3.13 shows that $\phi(\zeta)$ increases when Nt is increased.

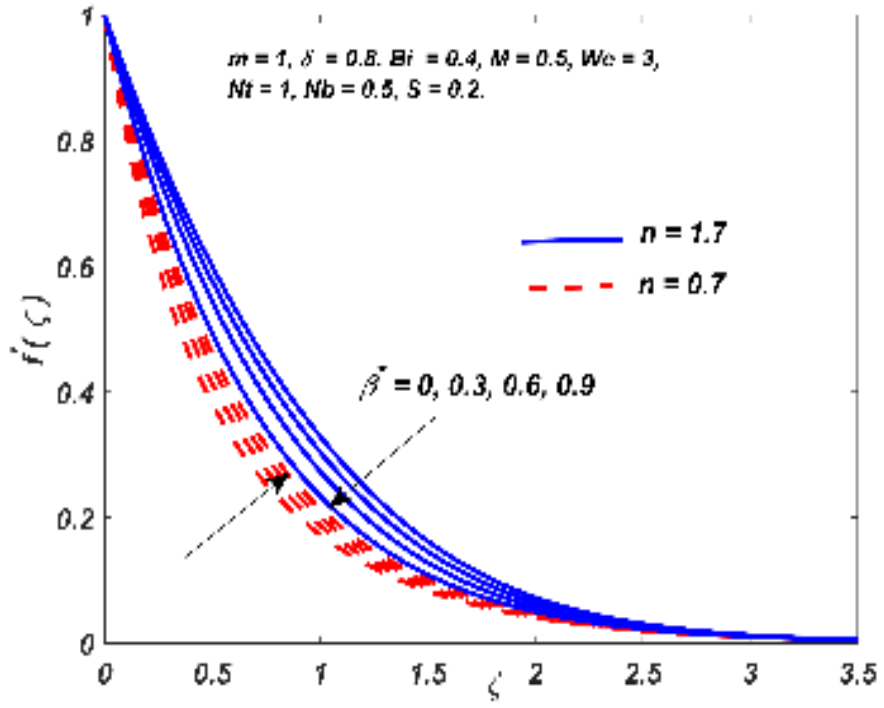

Figure 3.2: *Variation of* $f'(\zeta)$ *for various values of* β^*

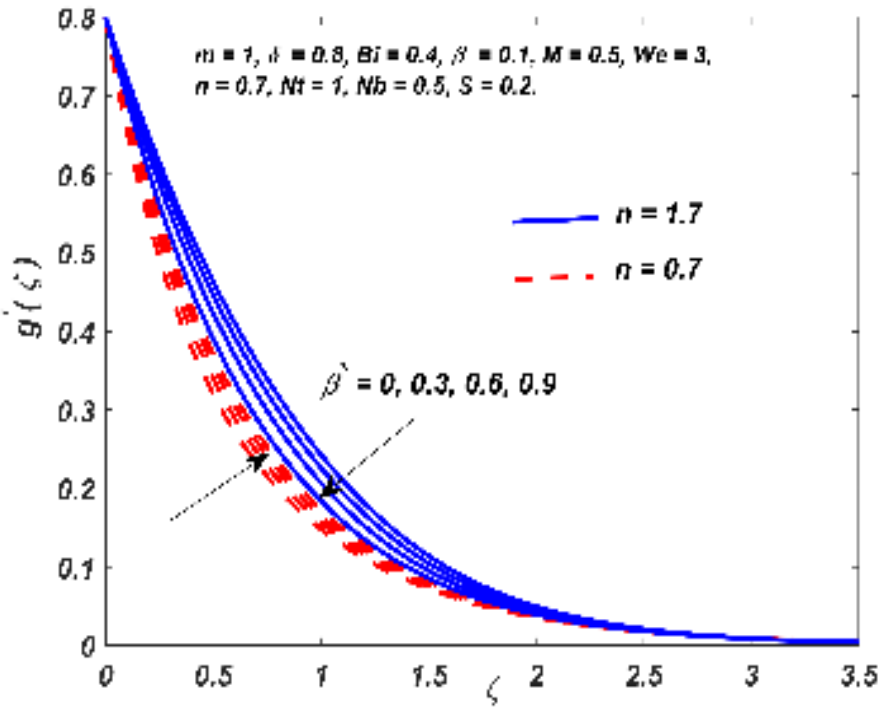

Figure 3.3: *Variation of* $g'(\zeta)$ *for various values of* β^*

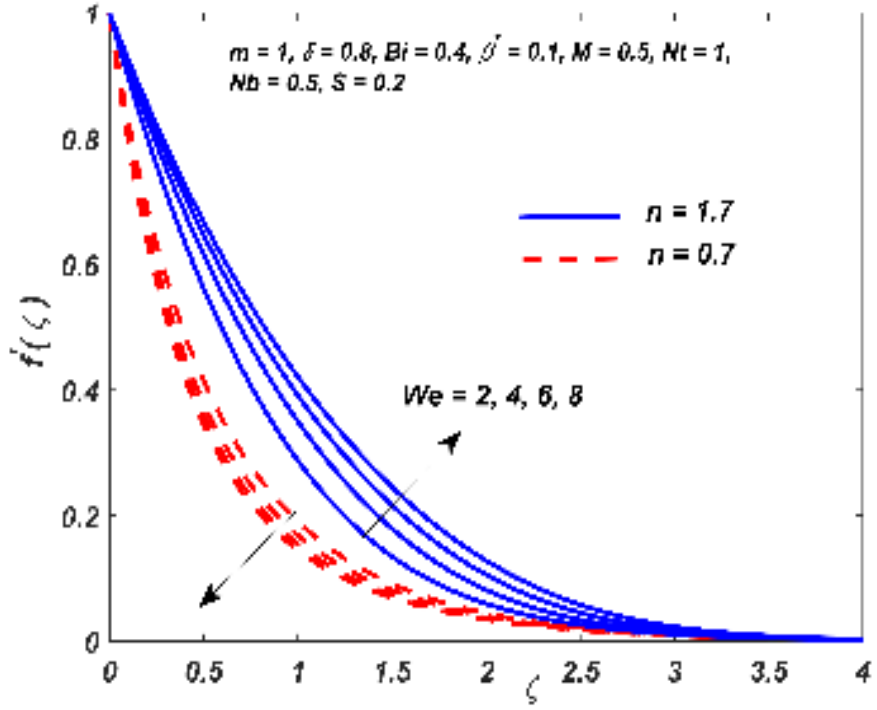

Figure 3.4: *Variation of* $f'(\zeta)$ *for various values of* We

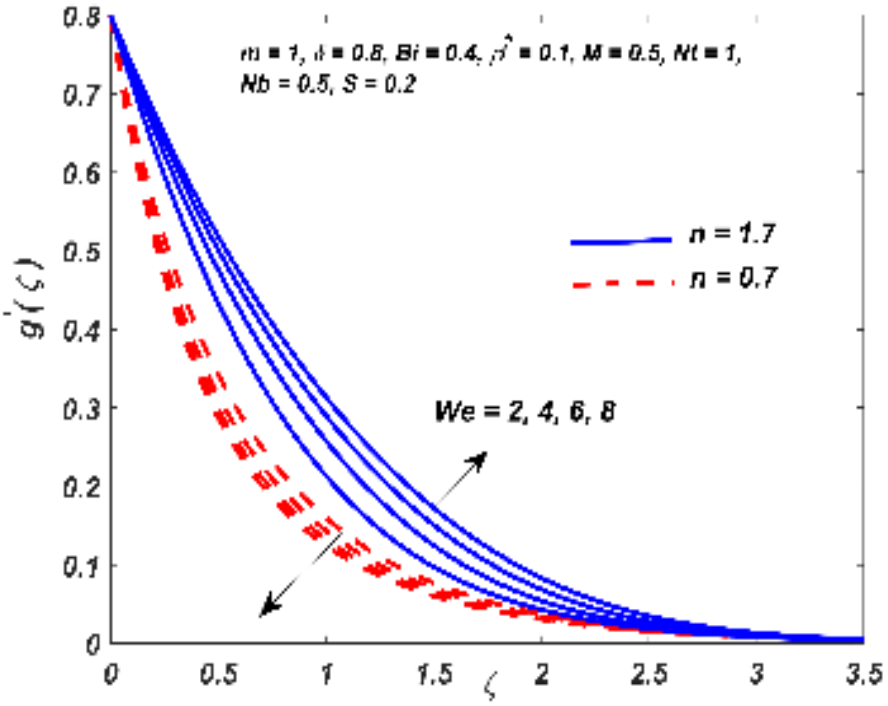

Figure 3.5: *Variation of* $g'(\zeta)$ *for various values of* We

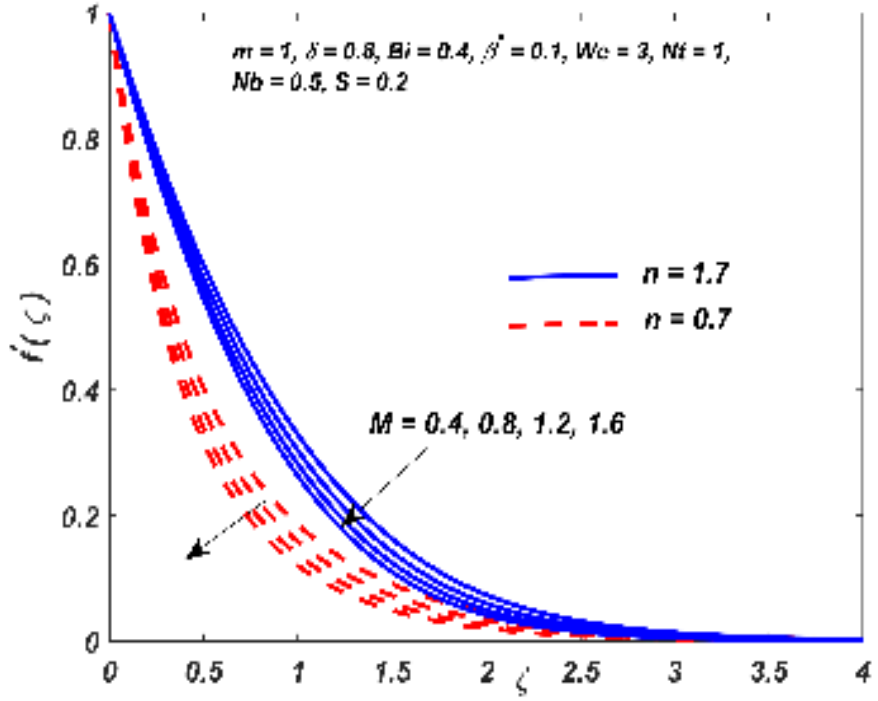

Figure 3.6: *Variation of* $f'(\zeta)$ *for various values of* M

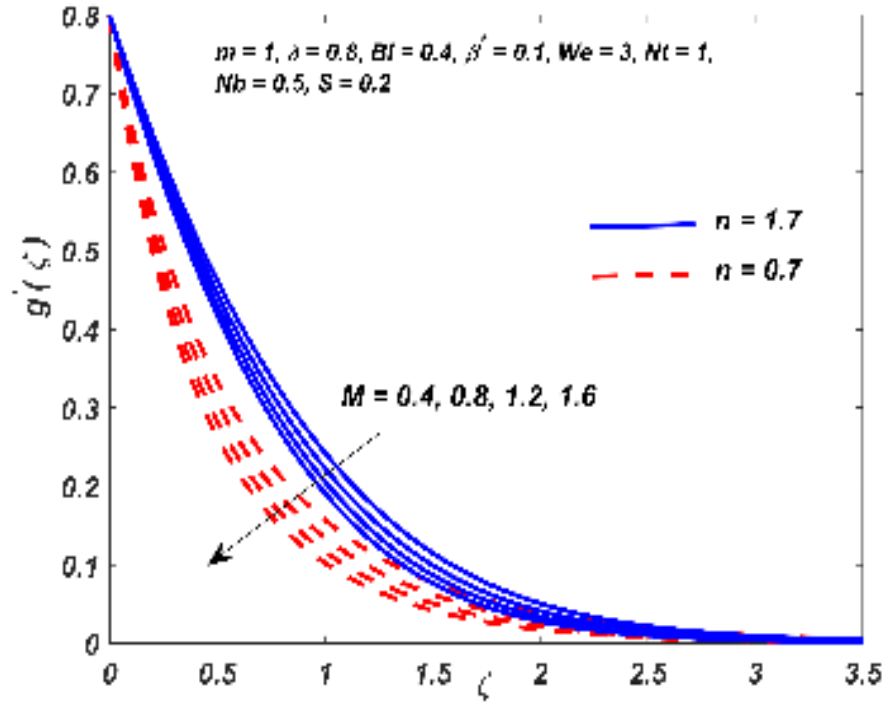

Figure 3.7: *Variation of* $g'(\zeta)$ *for various values of* M

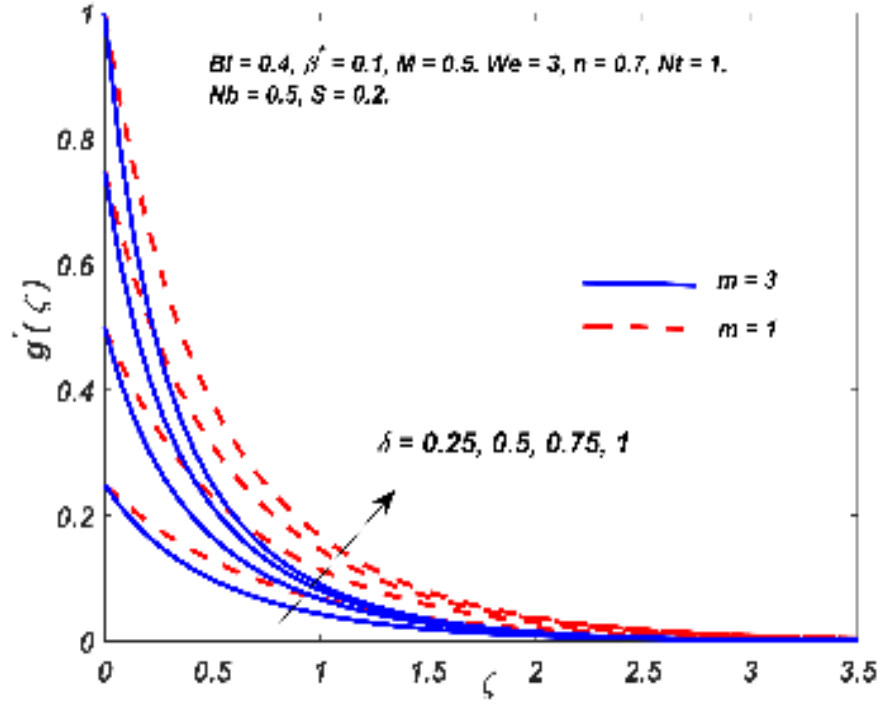

Figure 3.8: *Variation of* $g'(\zeta)$ *for various values of* δ

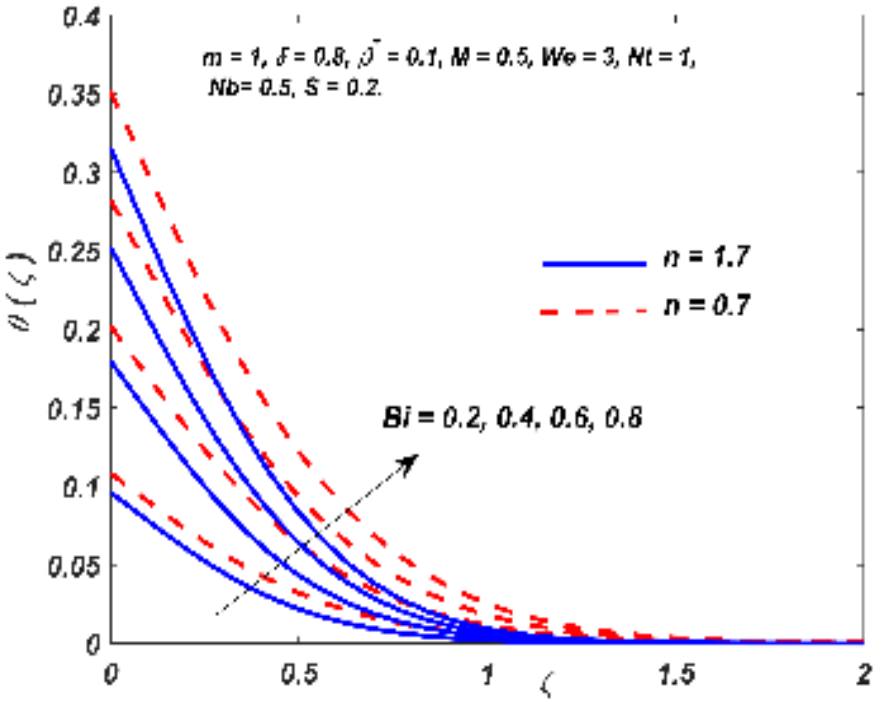

Figure 3.9: *Variation of* $\theta(\zeta)$ *for various values of* Bi

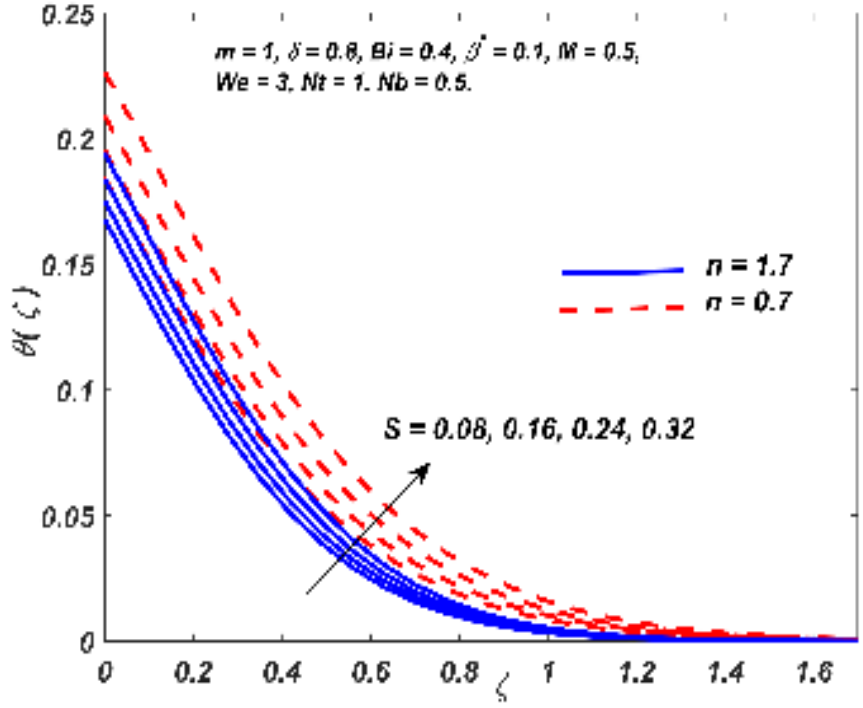

Figure 3.10: *Variation of* $\theta(\zeta)$ *for various values of* S

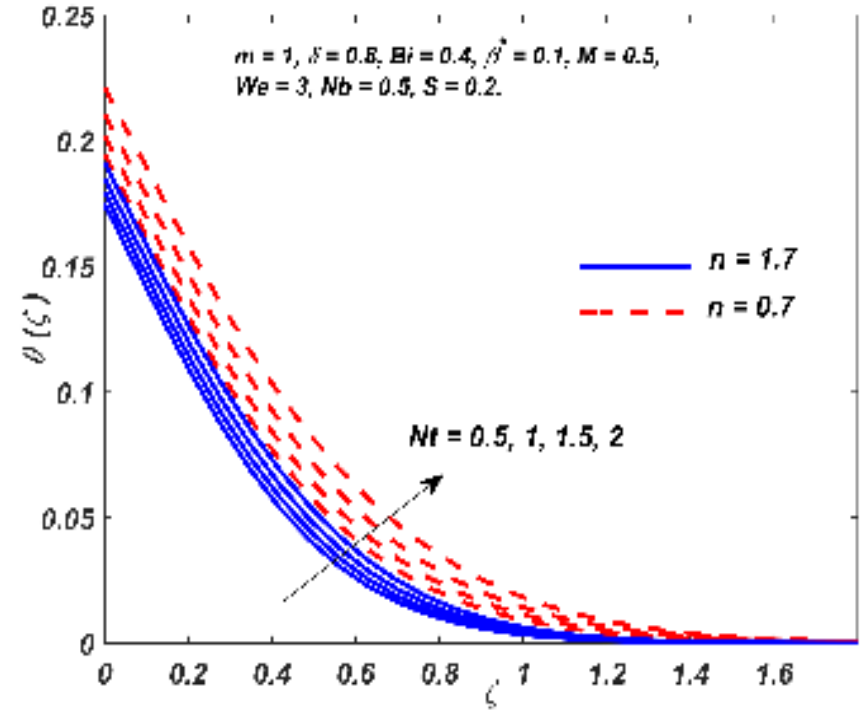

Figure 3.11: *Variation of* $\theta(\zeta)$ *for various values of* Nt

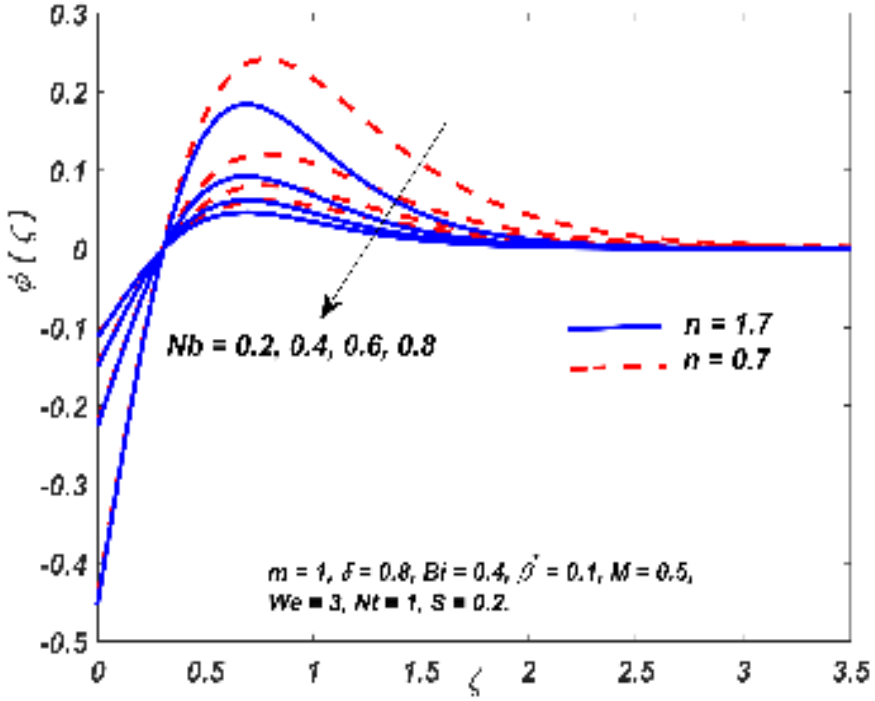

Figure 3.12: *Variation of $\phi(\zeta)$ for various values of Nb*

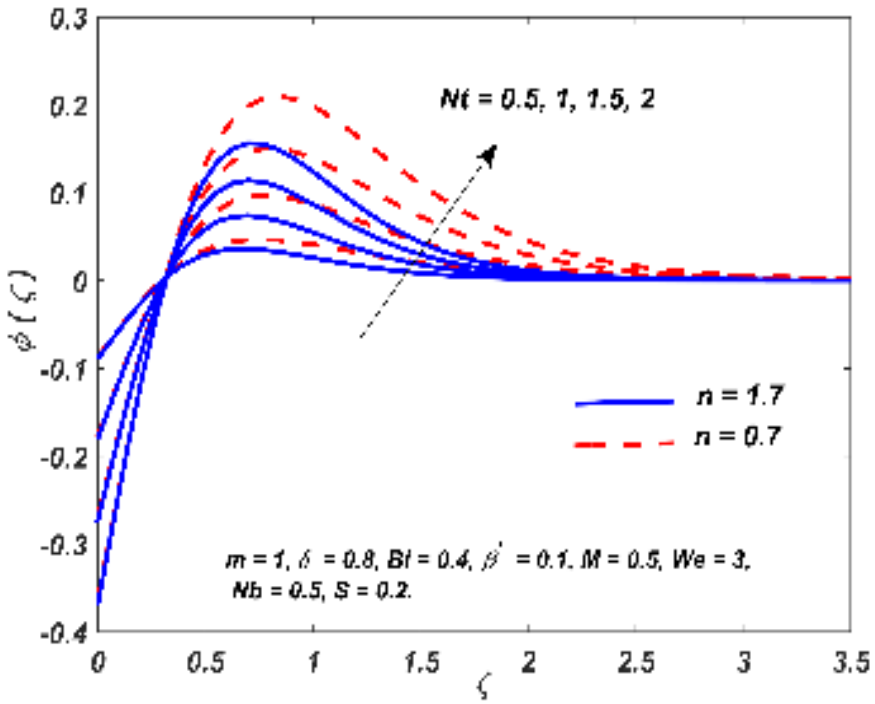

Figure 3.13: *Variation of $\phi(\zeta)$ for various values of Nt*

The effect of various parameters on local Nusselt number for $n = 0.7$ *and* 1.7 is studied using table 3.3. Increment/decrement rate denotes the percentage change of current value with respect to the previous value of local Nusselt number. A positive sign represents an increment while a negative sign represents decrement in heat transfer rate. From table 3.3, it is deduced that $Re_x^{-\frac{1}{2}} Nu$ (*both cases*) increases with δ and decreases for $Nt,\ S\ \&\ M$. It is further noted that $Re_x^{-\frac{1}{2}} Nu\ (n = 0.7)$ increases with β^* and decreases with We whereas the results are reversed for $Re_x^{-\frac{1}{2}} Nu\ (n = 1.7)$. Slope of linear regression is used to study the trend of variation in skin friction coefficient. A negative slope with respect to a parameter indicates that the parameter has a negative effect on skin friction meaning, an increase in that parameter will diminish the surface drag. Magnitude of slope represents the rate of change of skin friction coefficient per unit value of the corresponding parameter. The impact of various parameters on skin friction coefficients for $m = 1 \quad \& \quad 3$ at $n = 0.7 \quad \& \quad 1.7$ is illustrated in table 3.4 and 3.5.

From tables 3.4 and 3.5, it is inferred that We has a positive and negative impact on both skin friction coefficients $\left\{ Re_x^{\frac{1}{2}} Cf_x \quad \& \quad Re_y^{\frac{1}{2}} Cf_y \right\} (m = 1 \quad \& \quad m = 3)$ when $n = 0.7 \quad \& \quad 1.7$, respectively and β^* has a reversed impact on skin friction coefficients when compared with We. It is observed that M has a reducing effect on the surface drag. It is also observed that the skin friction coefficient decreases with increasing δ (for $Re_x^{\frac{1}{2}} Cf_x$) and increases with increasing δ (for $Re_y^{\frac{1}{2}} Cf_y$). The respective rate of change (slope) for each parameters are shown in tables 3.4 and 3.5.

3.5 Statistical Analysis

Statistical techniques like correlation and regression are widely used by researchers to identify the nature of impact of independent variables (various parameters) on the dependent variable (physical quantities like Nusselt number, drag coefficient or Sherwood number). Regression analysis helps in quantifying the variation of dependent variable due to the change in independent variables. Regression analysis eliminates the need for solving the problem repeatedly and thereby simplifying the calculation process. An approximate value of dependent variable can be faultlessly predicted for the chosen range of independent variables.

Table 3.3: *Variation in local Nusselt number at* $\zeta = 0$ *when* $m = 1$, $Nt = 1$, $S = 0.2$, $M = 0.5$, $We = 3$, $\delta = 0.8$, $\beta^* = 0.1$, $Nb = 0.5$ *and* $Bi = 0.4$

Nt	S	M	δ	We	β^*	$Re_x^{-\frac{1}{2}} Nu$		Increment Rate	
						$n = 0.7.$	$n = 1.7$	$n = 0.7$	$n = 1.7.$
0.5						0.3220801	0.3299969		
0.875						0.3199708	0.3286018	-0.655%	-0.423%
1.25						0.3175703	0.3270705	-0.750%	-0.466%
1.625						0.3147927	0.325376	-0.875%	-0.518%
2						0.3115088	0.3234827	-1.043%	-0.582%
	0.08					0.326205	0.3327401		
	0.14					0.32297	0.3305449	-0.992%	-0.660%
	0.2					0.3192066	0.3281077	-1.165%	-0.737%
	0.26					0.3147406	0.3253792	-1.399%	-0.832%
	0.32					0.3092984	0.3222934	-1.729%	-0.948%
		0.4				0.319804	0.3282712		
		0.7				0.3180105	0.3277891	-0.561%	-0.147%
		1				0.3162062	0.3273291	-0.567%	-0.140%
		1.3				0.3143798	0.3268877	-0.578%	-0.135%
		1.6				0.3125207	0.3264619	-0.591%	-0.130%
			0.25			0.2972953	0.3094536		
			0.4375			0.3071497	0.3172612	3.315%	2.523%
			0.625			0.3141479	0.3234272	2.278%	1.944%
			0.8125			0.3195285	0.3284102	1.713%	1.541%
			1			0.3238713	0.3325305	1.359%	1.255%
				2		0.320498	0.3271069		
				3.5		0.3186733	0.3284715	-0.569%	0.417%
				5		0.3173661	0.3292629	-0.410%	0.241%
				6.5		0.3163448	0.3297959	-0.322%	0.162%
				8		0.3155017	0.3301881	-0.266%	0.119%
					0.1	0.3192066	0.3281077		
					0.3	0.3205573	0.3276043	0.423%	-0.153%
					0.5	0.3216038	0.3269473	0.326%	-0.201%
					0.7	0.3224475	0.3260304	0.262%	-0.280%
					0.9	0.3231473	0.3245935	0.217%	-0.441%

3.5.1 Correlation and Probable Error

Correlation is a statistical technique which helps in determining the degree of relationship between two variables. The sign of correlation coefficient (r_c) determines the nature of relationship while magnitude of r_c indicates the magnitude of the relationship. Positive value of correlation coefficient implies that an increase in independent variable will fuel an increase in the dependent variable and negative value of correlation coefficient indicates that an increase in independent variable

Table 3.4: *Variation in Skin Friction Coefficients at* $\zeta = 0$ *when* $m = 1$, $Nt = 1$, $S = 0.2$, $M = 0.5$, $We = 3$, $\delta = 0.8$, $\beta^* = 0.1$, $Nb = 0.5$ *and* $Bi = 0.4$

We	β^*	M	δ	$-Re_x^{\frac{1}{2}} Cf_x$		$-Re_y^{\frac{1}{2}} Cf_y$	
				$n = 0.7$	$n = 1.7$	$n = 0.7$	$n = 1.7$
2				1.33511	1.86889	1.52449	2.02782
4				1.22088	2.15347	1.39943	2.32086
6				1.1555	2.36256	1.32533	2.54024
8				1.11123	2.52993	1.2746	2.71707
Slope				-0.03685	0.10961	-0.04119	0.11436
	0.2			1.30295	1.98544	1.48571	2.14815
	0.4			1.365	1.90031	1.54612	2.06399
	0.6			1.42028	1.80114	1.60037	1.9667
	0.8			1.47045	1.67999	1.64987	1.84939
Slope				0.27889	-0.50776	0.27337	-0.49678
		0.4		1.24376	1.97236	1.42361	2.13213
		0.8		1.33935	2.17465	1.53495	2.34492
		1.2		1.42665	2.3659	1.63649	2.54627
		1.6		1.50737	2.54804	1.73028	2.73812
Slope				0.21953	0.47958	0.25539	0.50483
			0.25	1.12977	1.70474	2.51655	2.89424
			0.5	1.19716	1.84841	1.81195	2.36941
			0.75	1.25722	1.99478	1.49662	2.20445
			1	1.31215	2.14103	1.31215	2.14103
Slope				0.24288	0.58209	-1.57142	-0.96983

will reduce the dependent variable. The reliability of the calculated correlation coefficient values is guaranteed using probable error (PE). Correlation is said to be significant (Fisher et al., 1921) if $\left|\frac{r_c}{PE}\right| > 6$; where $PE = \left(\frac{1-{r_c}^2}{\sqrt{\tilde{n}}}\right) 0.6745$ and $\tilde{n}$ is the number of observations.

From table 3.6, it is inferred that $Re_x^{-\frac{1}{2}} Nu$ (*both cases*) is positively correlated with δ and negatively correlated with S , M and Nt. It is observed that We exhibits negative and β^* exhibits positive correlation for $Re_x^{-\frac{1}{2}} Nu$ $(n = 0.7)$. It is also noted that the nature of correlation for We and β^* is reversed when $Re_x^{-\frac{1}{2}} Nu$ $(n = 1.7)$. Using $\left|\frac{r}{PE}\right|$ values, it can be concluded that all parameters of $Re_x^{-\frac{1}{2}} Nu$ (*both cases*) are significant.

Table 3.5: *Variation in Skin Friction Coefficients at* $\zeta = 0$ *when* $m = 3$, $Nt = 1$, $S = 0.2$, $M = 0.5$, $We = 3$, $\delta = 0.8$, $\beta^* = 0.1$, $Nb = 0.5$ *and* $Bi = 0.4$

We	β^*	M	δ	$-Re_x^{\frac{1}{2}} Cf_x$		$-Re_y^{\frac{1}{2}} Cf_y$	
				$n = 0.7$	$n = 1.7$	$n = 0.7$	$n = 1.7$
2				1.91894	3.054	2.1954	3.30479
4				1.74778	3.56384	2.00299	3.83948
6				1.65419	3.92644	1.89571	4.2241
8				1.59169	4.21322	1.82361	4.52954
Slope				-0.05377	0.19201	-0.06113	0.20294
	0.2			1.88497	3.25976	2.14958	3.52184
	0.4			2.00493	3.09201	2.2704	3.35199
	0.6			2.11052	2.89401	2.37747	3.15268
	0.8			2.20561	2.64641	2.47432	2.9061
Slope				0.53376	-1.01903	0.54065	-1.02327
		0.4		1.80207	3.29733	2.06412	3.55888
		0.8		1.86302	3.44808	2.13524	3.7165
		1.2		1.9213	3.59477	2.20316	3.87005
		1.6		1.97723	3.73779	2.26826	4.01989
Slope				0.14593	0.36702	0.17009	0.38415
			0.25	1.58658	2.71252	3.59345	4.50058
			0.5	1.69935	2.9938	2.58371	3.81117
			0.75	1.79885	3.27865	2.14315	3.61699
			1	1.88932	3.56095	1.88932	3.56095
Slope				0.40309	1.13206	-2.22118	-1.20522

Table 3.6: *Correlation Coefficient* (r_c)*, Probable Error* (PE) *and* $\left|\frac{r_c}{PE}\right|$ *of reduced Nusselt number at* $\zeta = 0$ *when* $Bi = 0.4$ *and* $Nb = 0.5$

Parameter	$Re_x^{-\frac{1}{2}} Nu$ when $n = 0.7$			$Re_x^{-\frac{1}{2}} Nu$ when $n = 1.7$		
	r_c	PE	$\left\|\frac{r_c}{PE}\right\|$	r_c	PE	$\left\|\frac{r_c}{PE}\right\|$
S	-0.9947	0.0032	311.6281	-0.9977	0.0014	732.2152
M	-1	0	63550.21	-0.9997	0.0002	5508.991
δ	0.9866	0.008	122.7986	0.992	0.0048	207.3562
We	-0.9879	0.0072	136.5306	0.9689	0.0185	52.4026
β^*	0.9915	0.0051	194.3342	-0.978	0.0131	74.4632
Nt	-0.9962	0.0023	430.4705	-0.9982	0.0011	909.9878

3.5.2 Multiple Linear Regression

Regression analysis is a statistical modelling technique used to establish a relationship between a dependent (Nusselt number) and one or more independent (various parameters considered) variables. Local Nusselt number for $n = 0.7$ and 1.7 is estimated using multiple linear regression models (as all correlations are significant). The estimated models are:

$$Nu_{est}^{n=0.7} = -0.07007S - 0.00566M + 0.03556\delta - 0.00072We + 0.00583\beta^* \\ -0.00697Nt + 0.31579 \tag{3.5.1}$$

$$Nu_{est}^{n=1.7} = -0.04343S - 0.00128M + 0.03116\delta + 0.00051We - 0.00352\beta^* \\ -0.00428Nt + 0.31540 \tag{3.5.2}$$

The accuracy of the estimated regression model is illustrated using Fig. 3.14 and 3.15. It is conclusive that δ and β^* have a positive impact whereas $S,\ M,\ We\ and\ Nt$ have negative impact on Nusselt number when $n = 0.7$. It can also be concluded that δ and We have a positive impact while $S,\ M,\ \beta^*\ and\ Nt$ have negative impact on Nusselt number when $n = 1.7$. This is in agreement with the results seen in table 3.3.

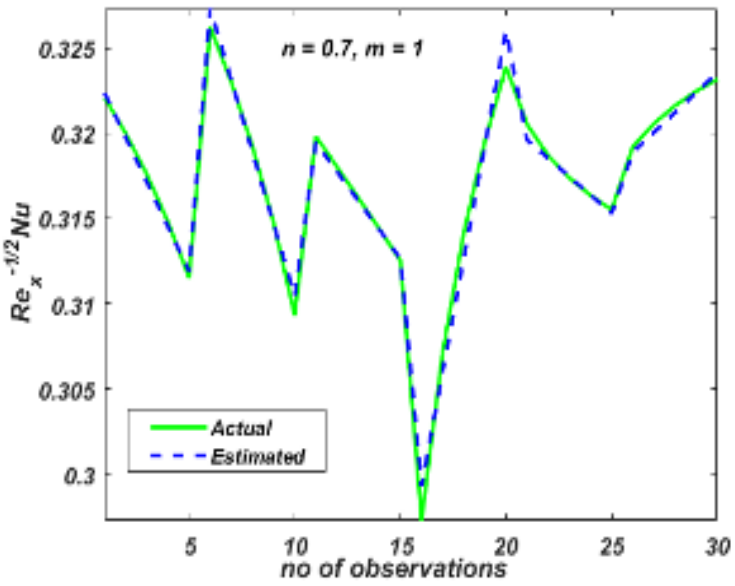

Figure 3.14: *Actual and estimated values* $Re_x^{-\frac{1}{2}}\ Nu$ *of when* $n = 0.7$

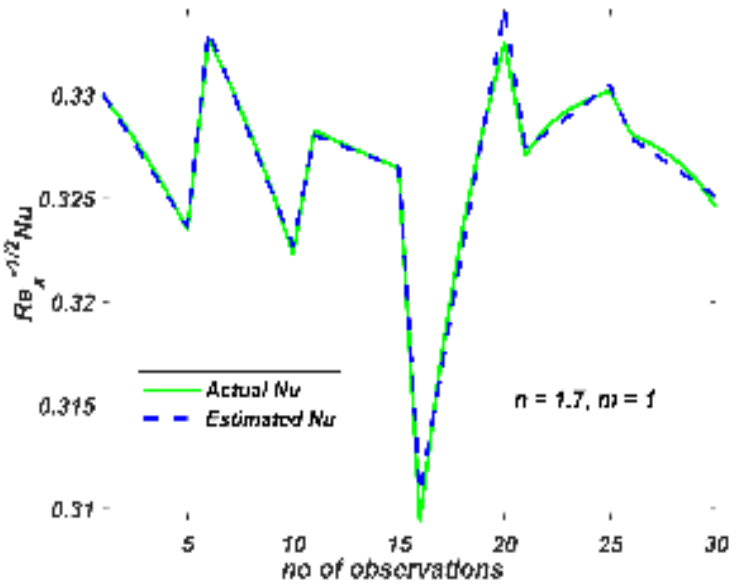

Figure 3.15: *Actual and estimated values* $Re_x^{-\frac{1}{2}}\ Nu$ *of when* $n = 1.7$

3.6 Conclusions

The major conclusions drawn from the current analysis are given below:

- The velocity profiles are directly proportional to the viscosity ratio parameter in shear thinning case and inversely proportional in shear thickening case.
- Weissenberg number enhances the velocity profiles in case of shear thickening fluids and retards the velocity profiles for shear thinning fluids.
- An exponential increase is observed in the temperature profile due to an increase in Biot number, heat generation/absorption and thermophoresis parameters.
- Hartmann number has a destructive effect on surface drag and the velocity profiles.
- Increase in the stretching ratio parameter improves the Y directional velocity profile.
- The concentration profile is enhanced and depleted with increasing thermophoresis and Brownian motion effects, respectively.
- The regression models are found to be in synchronization with the numerical results for the chosen values of parameters.